Author(s): Qi, Jiaran & Kettunen, Henrik & Wallén, Henrik & Sihvola, Ari

Title: Different homogenization methods based on scattering parameters of dielectric-composite slabs

Year: 2011

Version: Final published version

Please cite the original version:

Qi, Jiaran & Kettunen, Henrik & Wallén, Henrik & Sihvola, Ari. 2011. Different homogenization methods based on scattering parameters of dielectric-composite slabs. Radio Science. Volume 46, Issue 5. RS0E08/1-7. 1944-799X (electronic). 0048-6604 (printed). DOI: 10.1029/2010RS004622.

Different homogenization methods based on scattering parameters of dielectric-composite slabs

Jiaran Qi,[1] Henrik Kettunen,[1] Henrik Wallén,[1] and Ari Sihvola[1]

Received 21 December 2010; revised 29 March 2011; accepted 4 May 2011; published 11 August 2011.

[1] The dispersion of the effective permittivity of a dielectric-composite slab is analyzed in a quasi-dynamic range using the simulated transmission and reflection data from the slab illuminated by an obliquely incident plane wave. Based on the retrieval results, the procedure for finding the dynamic trust region of the quasi-static Lord Rayleigh estimate for the effective permittivities of such composites is then developed. According to this process, the upper frequency limit of this trust region is numerically determined by an interpolation function. The proposed function of the inclusion area fraction p and relative permittivity ε_i is demonstrated as a good predictor within the ranges $0.1 \le p \le 0.5$ and $10 \le \varepsilon_i \le 60$. It is further shown that within the above ranges the effective wavelength inside the material should be at least 33 times the edge length of the unit cell, in order to ensure that the defined relative difference between the retrieved effective permittivity and the quasi-static estimate is not larger than 1%.

Citation: Qi, J., H. Kettunen, H. Wallén, and A. Sihvola (2011), Different homogenization methods based on scattering parameters of dielectric-composite slabs, *Radio Sci.*, *46*, RS0E08, doi:10.1029/2010RS004622.

1. Introduction

[2] Macroscopic electromagnetic (EM) properties of composites and relevant characterization techniques are classical topics for researchers working in diverse disciplines and different frequency ranges [*Brosseau*, 2006; *Silveirinha*, 2007; *Mochan et al.*, 2010; *Galek et al.*, 2010]. Within the long-wavelength, or quasi-static, regime, homogenization theories, such as classic mixing formulas, were significantly advanced during the last one and a half centuries and systematically documented by, e.g., *Sihvola* [1999], *Milton* [2002], and *Weiglhofer and Lakhtakia* [2003]. On the other hand, many recently developed methods, such as scattering parameter (S parameter) retrieval, and various field averaging procedures [*Smith and Pendry*, 2006; *Fietz and Shvets*, 2010], make it possible to determine the dynamic EM properties of composites.

[3] Since originally proposed by *Nicolson and Ross* [1970] and *Weir* [1974], the S parameter retrieval has widely been applied in medium parameter extractions. *Smith et al.* [2002] reported the first extension of this method to determine the effective medium parameters of a metamaterial composed of an array of split ring resonators and short wires. *Chen et al.* [2004] further improved the robustness of the method for its application to a similar structure, with the focus on the branch selection and the medium-environment interface determination. Later on, the S parameter retrieval was generalized for bianisotropic media when only a particular polarization is considered [*Chen et al.*, 2005; *Li et al.*, 2009], and for isotropic reciprocal chiral media [*Wang et al.*, 2009].

[4] When lossless or low loss dielectric composites with finite thickness are considered, the problems related to the S parameter retrieval are, however, different, such as the distortion of the retrieval result by the Fabry-Pérot resonances (FPR) [*Sjöberg and Larsson*, 2010; *Qi et al.*, 2010a, 2010b]. More importantly, if the composites are assumed nonmagnetic and treated effectively homogenous, the effective permittivity can then be analyzed using both S parameters, either one of them, or only some special reflection data. We will in this paper generalize the four different retrieval methods by *Qi et al.* [2010a] to the case when a composite slab is illuminated by an obliquely incident plane wave. Although the homogenous model becomes physically less rigorous when the geometry details are not very small compared with the wavelength, a rather broad frequency range is considered to better show the intrinsic properties of different methods and the limitations regarding the homogenous model.

[5] Based on the retrieval results, the accuracy of the quasi-static Lord Rayleigh estimate for the effective permittivity of the composite is explored in a quasi-dynamic range by an interpolation-function method. The corresponding procedure is introduced, and the interpolation and extrapolation abilities of the developed function are evaluated. Moreover, we define a dynamic trust region using a limiting ratio between the effective wavelength inside the slab and the edge length of the unit cell. Above this ratio, the quasi-static esti-

[1]Department of Radio Science and Engineering, School of Electrical Engineering, Aalto University, Aalto, Finland.

0048-6604/11/2010RS004622

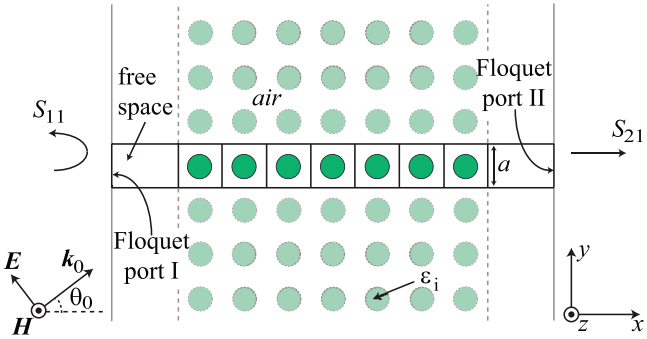

Figure 1. The quasi 2-D geometry setup of the considered composite slab. In CST MWS, we only construct one row of seven consecutive unit cells (the highlighted area).

mate can reasonably be used to describe the electric response of the composite.

2. Geometry Setup and Retrieval Methods

2.1. Dielectric-Composite Slab of Interest

[6] We consider in this paper a composite slab consisting of infinitely long dielectric circular cylinders with relative permittivity ε_i periodically distributed in vacuum ($\varepsilon_e = 1$). Due to translation invariance, such a composite can effectively be modeled in two dimensions (2-D). As shown in Figure 1, the unit cell of side length a is composed of an air background and a circular disc filling an area fraction p. The slab is then infinite in the y direction and contains seven layers of the unit cells in the x direction. Seven layers is a reasonable compromise between a large layer number which ensures the slab to behave like a homogeneous medium, and a small one which reduces the computational expenses and the number of thickness resonances.

[7] In order to determine the frequency dispersion of the effective permittivity of the slab on which a plane wave is obliquely incident, the full wave simulator CST Microwave Studio (CST MWS) is applied to construct the geometry above and to collect the required transmission and reflection data. In CST MWS, only the highlighted area in Figure 1 needs to be modeled. The composites can then be realized by assigning the unit cell boundary condition to the four bounds in the y and z directions. By applying the Floquet ports and further varying the phase shift between the y directional unit cell boundary pair, a plane wave with the incident angle θ_0 is achieved. Herein, only TM_{xy} polarization is considered, since the TE_{xy} polarization will not induce strong dipole interactions and the effective permittivity is just the area averaged result. Moreover, free space of two unit cells is added on each side of the slab to ensure that the fields collected by the ports are practically plane waves.

[8] As a three-dimensional tool, CST MWS cannot model a real 2-D structure. However, the z directional thickness d_z in this case only affects the simulation duration but does not introduce extra errors, as long as d_z is at least one-mesh-cell long so that the qualities of the tetrahedral mesh cells do not deteriorate. Thus, one can build a quasi 2-D structure, whose d_z is, for example, one-tenth of the side length a of the unit cell, in order to reduce the simulation duration without compromised accuracy.

2.2. Different Retrieval Methods Based on S Parameters at Oblique Incidence

2.2.1. Retrieval From Both S Parameters With Compensation Method

[9] Assuming that the composite slab can be effectively treated as a homogenous medium, the S parameters for an obliquely incident plane wave are

$$S_{11} = \frac{R\left(1 - e^{-j2k_0 d\cdot n\cos\theta_1}\right)}{1 - R^2 e^{-j2k_0 d\cdot n\cos\theta_1}}, \tag{1}$$

$$S_{21} = \frac{(1 - R^2)e^{-jk_0 d\cdot n\cos\theta_1}}{1 - R^2 e^{-j2k_0 d\cdot n\cos\theta_1}}, \tag{2}$$

$$R = \frac{z\cdot\cos\theta_1 - \cos\theta_0}{z\cdot\cos\theta_1 + \cos\theta_0}, \qquad \sin\theta_1 = \sin\theta_0/n, \tag{3}$$

where the time convention $\exp(j\omega t)$ is used, n and z are refractive index and impedance of the slab medium, θ_0 and θ_1 are the incident angle in the air and the effective refractive angle in the slab, k_0 is the free space wave number, and d denotes the slab thickness. To make the analytic inversion simpler, we define n' and z' as

$$n' = n\cos\theta_1 = \sqrt{\varepsilon_{\text{eff}}\mu_{\text{eff}}}\cos\theta_1, \tag{4}$$

$$z' = \frac{z\cos\theta_1}{\cos\theta_0} = \sqrt{\frac{\mu_{\text{eff}}}{\varepsilon_{\text{eff}}}}\frac{\cos\theta_1}{\cos\theta_0}. \tag{5}$$

Thus, we have similarly to the normal incident case by *Chen et al.* [2004]

$$z' = \pm\sqrt{\frac{(1 + S_{11})^2 - S_{21}^2}{(1 - S_{11})^2 - S_{21}^2}}, \tag{6}$$

$$n' = (k_0 d)^{-1}[j\ln(Q) + 2m\pi], \tag{7}$$

$$Q = \frac{S_{21}}{1 - S_{11}(z' - 1)(z' + 1)^{-1}}, \tag{8}$$

where the integer m is the branch index of the logarithmic function. Once z' and n' are determined, the effective relative permittivity ε_{eff} and the effective relative permeability μ_{eff} of the composite slab can be retrieved by

$$\varepsilon_{\text{eff}} = \frac{n'}{z'\cos\theta_0}, \qquad \mu_{\text{eff}} = \frac{n'z'\cos\theta_0}{\cos^2\theta_1}. \tag{9}$$

For a lossless or low loss dielectric composite slab, the retrieval results by (9) will, however, be severely distorted by the FPR due to the ill-defined impedance z' [*Sjöberg and Larsson*, 2010; *Qi et al.*, 2010a, 2010b]. On the other hand, n' does not suffer from the FPR. To eliminate the surprisingly broadband influence of the FPR and restore physically reasonable medium parameters, we can assume the magnetic response negligible, i.e., $\mu_{\text{eff}} = 1$, and thus retrieve ε_{eff} using

only n'. Based on the nonmagnetic assumption and (9), we have

$$\varepsilon_{\text{eff}} = \frac{n'^2 + \sin^2\theta_0}{\mu_{\text{eff}}}, \tag{10}$$

which is called the compensation method [*Qi et al.*, 2010b]. Moreover, the nonmagnetic assumption is quite reasonable for the considered frequency range and the dielectric composites with not very large permittivity contrasts, since the artificial magnetism is the second-order spatial dispersion effect in terms of the ratio between the unit cell dimension and the effective wavelength [*Landau and Lifshitz*, 1984].

2.2.2. S_{11} Method and S_{21} Method

[10] Moreover, both (1) and (2), with the nonmagnetic assumption, become functions of only one variable, i.e., ε_{eff}. We can thus retrieve ε_{eff} by numerically inverting either (1) or (2). In order to locate the complex roots of a nonlinear equation with complex coefficients, we numerically separate the equation into real and imaginary parts, and then solve a system of the two nonlinear yet real equations from the separation in a least square sense by the Levenberg-Marquardt algorithm [*Levenberg*, 1944].

2.2.3. Effective Wavelength Method

[11] As thickness resonances, FPR will appear when the effective slab thickness $d\cdot\cos\theta_1$ is equal to an integer multiple of half of the effective wavelength of the field inside the slab [*Qi et al.*, 2010a, 2010b]. At these frequencies, the cancelation of multireflection will lead S_{11} to be zero, which provides us the fourth way to determine ε_{eff} at these discrete frequencies. Thus from (1), we have $\exp(-j2k_0nd\cos\theta_1) = 1$, which yields

$$\varepsilon_{\text{eff}} = \left(\frac{r\lambda_r}{2d}\right)^2 + \sin^2\theta_0, \qquad r = 1, 2, 3, \ldots \tag{11}$$

where λ_r denotes the free space wavelength at the FPR of order r. Although only valid for discrete frequencies, the effective wavelength method (EWM) provides a good comparison for other retrieval results.

[12] It is worth to mention that $S_{11} = 0$ is not a sufficient condition for the applicability of the EWM at oblique incidence for the TM polarization, since R in (3) could also be zero. That corresponds to the definition of Brewster's angle [*Kong*, 2008]. Since the effective Brewster's angle may also be dispersive in the dynamic analysis, we should carefully sort out the FPR-related frequency points from all the zero-reflection frequencies when applying the EWM at the incident angles close to the static Brewster's one.

3. Retrieval Results

3.1. Static Lord Rayleigh Estimate and Normalized Frequency f/f_{20}

[13] For an infinite simple square lattice with the unit cell shown in Figure 1, the 2-D Lord Rayleigh mixing formula [*Rayleigh*, 1892] can accurately estimate the relative static ε_{eff} as

$$\varepsilon_{\text{Ray}} = \varepsilon_e + \frac{2p\varepsilon_e}{(\varepsilon_i + \varepsilon_e)(\varepsilon_i - \varepsilon_e)^{-1} - p - (\varepsilon_i - \varepsilon_e)(\varepsilon_i + \varepsilon_e)^{-1}(0.3058p^4 + 0.0134p^8)}. \tag{12}$$

For the finite-thickness slab of our interest, (12) could still supply a good reference to its static ε_{eff}. However, it was reported by *Simovski et al.* [2000] and numerically confirmed by *Kettunen et al.* [2010] that for such a slab the outermost boundary layers have slightly larger electric response than all the inner layers, whose permittivities are roughly identical, and converge to ε_{Ray} with the decreasing frequency. Therefore, the retrieved ε_{eff} is expected to converge to a value slightly larger than ε_{Ray} at low frequencies.

[14] Moreover, we normalize the frequency f according to a reference f_{20}, which is the frequency when the effective wavelength λ_{eff} inside the slab equals 20 times the length of the unit cell edge a. We then choose the 2-D Lord Rayleigh result ε_{Ray} as the static estimate for ε_{eff} of the composite slab, and reduce the free space wavelength λ_0 to ε_{Ray}, i.e., $\lambda_{\text{eff}} = \lambda_0/(\varepsilon_{\text{Ray}})^{1/2}$. The normalized frequency f/f_{20} can thus approximately indicate the ratio between a and λ_{eff}. For instance, a is one-tenth of λ_{eff} when f/f_{20} equals 2.

3.2. Comparison Among Different Retrieval Methods

[15] A composite slab with $\varepsilon_i = 10$ and $p = 0.2$ is considered in this section. The retrieved ε_{eff} by the introduced four methods, i.e., the both S parameters with compensation method (BSCM), the S_{11} method, the S_{21} method, and the EWM, at various θ_0 are compared. However, the comparison between results by (9) and (10), i.e., without and with the compensation approach, has been thoroughly discussed by *Qi et al.* [2010a, 2010b], and is not included herein.

[16] It is shown in Figure 2 that the retrieved results by the BSCM for $\theta_0 = 0°$, 30°, 45°, and 60° converge as expected to a value slightly larger than the static Rayleigh estimate ε_{Ray} at very low frequency. With the increasing frequency, all the results gradually grow and deviate from one another due to spatial dispersion. Meanwhile, the S_{21} method predicts globally a similar dispersion at each θ_0, although it fails to display the expected low-frequency convergence. It should be noted that although these two methods yield similar results, they are intrinsically different in that the BSCM uses both S parameters to arrive at (10), while the S_{21} method only uses S_{21}. It is, moreover, shown in Figure 2b that ε_{eff} retrieved by the EWM has good agreement at 0°, 30°, and 60° with those by the BSCM and by the S_{21} method, except for $\theta_0 = 45°$, where larger deviations are observed. It is because in this case θ_0 is very close to the static Brewster's angle (49.2°), so that the field is weakly reflected, i.e., $S_{11} \approx 0$. The simulation errors in S_{11} thus have more crucial influence.

[17] Figure 3 shows that for $\theta_0 = 0°$, 30°, 45°, and 60°, the discrete permittivities retrieved by the EWM agree exactly with those by the S_{11} method. It is because both methods attempt to characterize the medium based on only S_{11}, and the EWM is thus a special case of the S_{11} method. More importantly, the S_{11} method seems less stable than the BSCM and the S_{21} method, since it fails to present a monotonically increasing dispersion. This is due to the fact that for small $p = 0.2$, moderate $\varepsilon_i = 10$, and not very large θ_0, S_{11} is close to zero. Hence, poor stability of the S_{11} method is expected. This fact also explains why the S_{11} method fails at

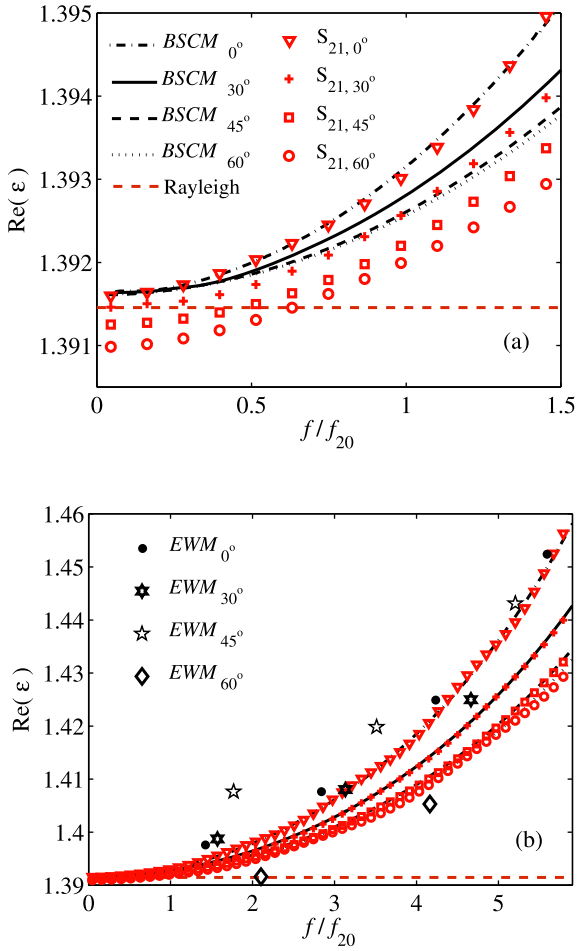

Figure 2. Comparison among the retrieved effective permittivities by different S parameter retrieval methods at various incident angles. (a) Low frequency comparison between the BSCM and the S_{21} method at $\theta_0 = 0°$, 30°, 45°, and 60°. (b) Global comparison among the BSCM, the S_{21} method, and the EWM.

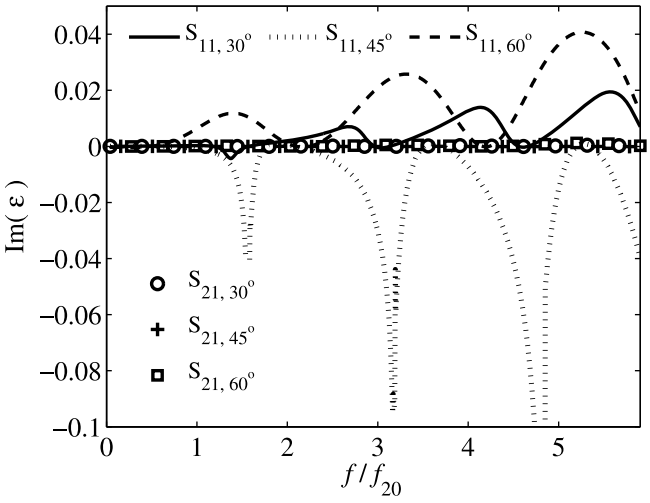

Figure 4. Comparison between the imaginary parts of the retrieved permittivities by the S_{11} method and the S_{21} method at $\theta_0 = 30°$, 45°, and 60°.

$\theta_0 = 45°$ close to the static Brewster's angle. In this case, S_{11} is practically zero which leads to a nearly resonating real part of the ε_{eff} as well as a negative imaginary part in Figure 4. On the other hand, Figure 4 also shows that the imaginary parts of the retrieved ε_{eff} by the S_{21} method are practically zero compared with those by the S_{11} method at $\theta_0 = 30°$, 45°, and 60°, which also indicates that the S_{21} method is superior to the S_{11} method for moderately oblique incidence. In addition, despite of the sign difference, the nonzero imaginary parts by the S_{11} method are not reasonable since our dielectric composite slabs are lossless and passive.

[18] Nevertheless, for very large θ_0, larger reflection will be encountered so that the stabilities of the S_{11} method and the EWM are expected to improve while the S_{21} method deteriorates. Figure 5 demonstrates this point. It is also found that the dispersion of the retrieved ε_{eff} at 75° by the BSCM is above that at 60° and very close to that at 45°. As reported by

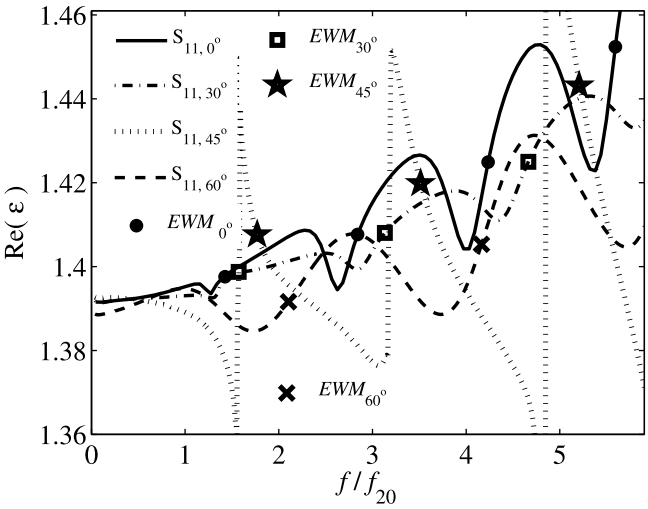

Figure 3. Comparison between the S_{11} method and the EWM at $\theta_0 = 0°$, 30°, 45°, and 60°.

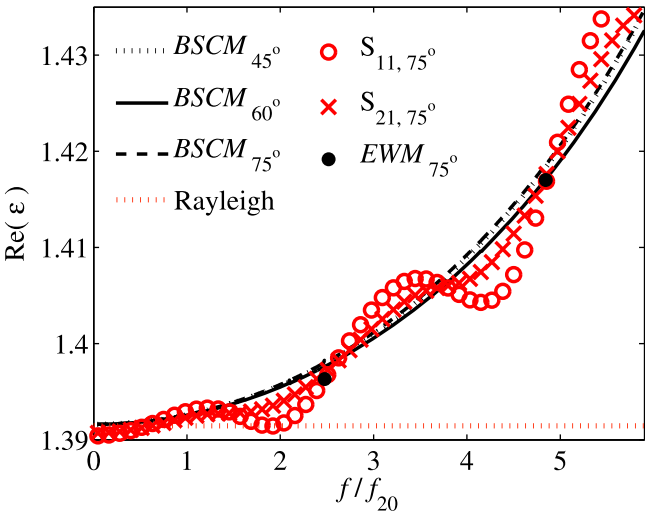

Figure 5. The comparison among different retrieval methods at a very large θ_0 (= 75°).

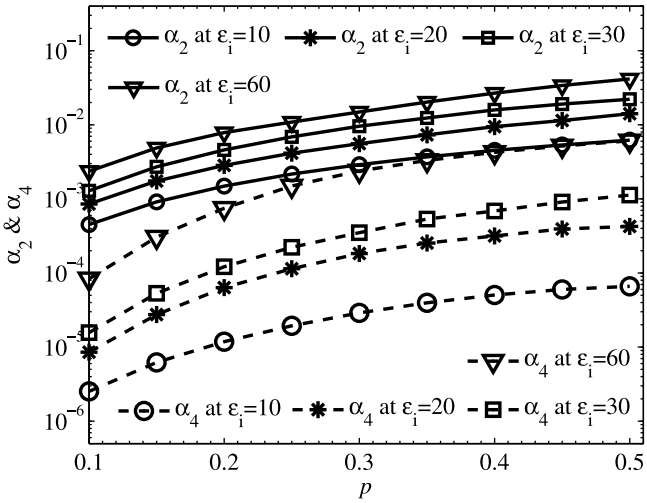

Figure 6. Comparison between the values of the coefficients α_2 and α_4 of (13).

McPhedran et al. [1996], the lowest dispersion curve is expected at $\theta_1 = 45°$ for an infinite simple square lattice, which inherits the diagonal symmetry of the unit cell. When a slab with the same unit cell is instead considered, we can predict by Snell's law that the corresponding θ_0 is around 60°.

[19] Finally, the BSCM is superior to the other homogenization methods according to the following criteria. First, a proper homogenization is to build an effective medium with physically reasonable parameters rather than reproduce the S parameters. More precisely, the goal of homogenizing a heterogeneous structure is to describe its intrinsic EM properties by a modeled bulk medium with effective medium parameters. To this end, the effective medium parameters should display reasonable dispersion and not violate fundamental physical laws. Due to the simple geometry of the considered composites, its dispersion, close to the quasi-static limit, is expected to behave like a smoothly increasing curve without any bumps or discontinuities. Second, the difference between S parameters from the homogeneous model and from the original structure is a good measure of the homogenization methods. We thus define a sum criterion $\Delta S_{total} = |\Delta S_{11}| + |\Delta S_{21}|$ to assess the errors arisen from different methods. It turns out that although the BSCM introduces errors into both S parameters, it clearly leads to smaller ΔS_{total} than the S_{11} method. In addition, the S_{21} method seems to produce the same-level errors compared with the BSCM, but its stability deteriorates for large θ_0 as shown in Figure 5. In all, the BSCM is the best choice compared with the other methods for the considered composite slab, because it not only restores physically meaningful dispersive ε_{eff}, but also generates least errors measured by the sum criterion ΔS_{total}.

4. Quasi-Static Limit for the Composite Slab: An Interpolation Method

[20] In section 3.2, different retrieval methods have been compared, and the BSCM turns out to be the most robust technique to characterize the dielectric composite slab shown in Figure 1. The dispersive ε_{eff} gradually deviates from the static Lord Rayleigh result as shown in Figure 2, which implies that the accuracy of the quasi-static estimate describing the electric response of the slab is reduced when the frequency grows. It is, therefore, important to find the dynamic trust region of the quasi-static estimate for the considered slabs with different p and ε_i by defining a proper criterion.

[21] To quantify this problem, we define the relative difference between ε_{Ray} and the retrieved ε_{eff} as $(\varepsilon_{eff} - \varepsilon_{Ray})/\varepsilon_{Ray}$, and choose 1% relative difference as a satisfactory tolerance. We further define the limit frequency meeting this criterion as f_L, and thus the normalized upper frequency limit of the dynamic trust region of the quasi-static estimate is denoted as f_L/f_{20}. Below this limit, the largest relative deviation $\Delta\varepsilon/\varepsilon_{Ray}$ among the retrieved ε_{eff} at various θ_0, is also less than the 1% tolerance. Spatial dispersion can thus be neglected. We will hereafter express f_L/f_{20} as a function of the inclusion area fraction p and relative permittivity ε_i.

[22] To build the desired function, the first step is to repeat the full wave simulation and the retrieval by the BSCM for different p and ε_i to collect sufficient data for the fitting purpose. Only the normal incidence needs to be considered since it displays the largest deviation from ε_{Ray}. In particular, we choose values of 10, 20, 30, and 60 for ε_i, and for each ε_i, 9 samples from 0.1 to 0.5 are assigned to p.

[23] The next step is, for each combination of the above p and ε_i, to numerically fit the retrieved dispersive ε_{eff} using a function of f/f_{20}. As suggested by *McPhedran et al.* [1996], we construct the function by adding two higher-order correction terms to the static one,

$$\varepsilon_{eff} = \alpha_0 + \alpha_2 \cdot (f/f_{20})^2 + \alpha_4 \cdot (f/f_{20})^4, \tag{13}$$

where α_0 is the static estimate term, the quadratic term denotes the electric quadrupole and the magnetic dipole corrections, and the fourth-power term considers higher-order multipole interactions. The coefficients α_0, α_2, and α_4 are then determined using the MATLAB curve fitting tool. We thus have 36 data points for each coefficient in (13).

[24] The following step is to numerically fit each coefficient in (13) using a function of p and ε_i. It is, however, noted from Figure 6 that α_4 is at least one order of magnitude smaller than the corresponding α_2. Since f_L/f_{20} is of our interest, the first and the second terms in (13) are expected to be the leading contributions. We, therefore, truncate (13) to consider only the static and the quadratic terms. For α_0, we use a fitting function based on the Lord Rayleigh formula; for α_2, we choose a polynomial function of p and ε_i, because better fitting functions, whose constituent terms have obvious physical interpretations, are not readily available. The MATLAB surface fitting tool is then applied to optimize the coefficients of these fitting functions in a least square sense. The applied fitting functions, denoted as α_0' and α_2', and their optimized coefficients are shown in Appendix A.

[25] We have up to now established the interpolation function to approximate the dispersive ε_{eff} of the composite slab with $0.1 < p < 0.5$ and $10 < \varepsilon_i < 60$, which reads

$$\varepsilon_{eff}(f/f_{20},\ p,\ \varepsilon_i) = \alpha_0' + \alpha_2' \cdot (f/f_{20})^2, \tag{14}$$

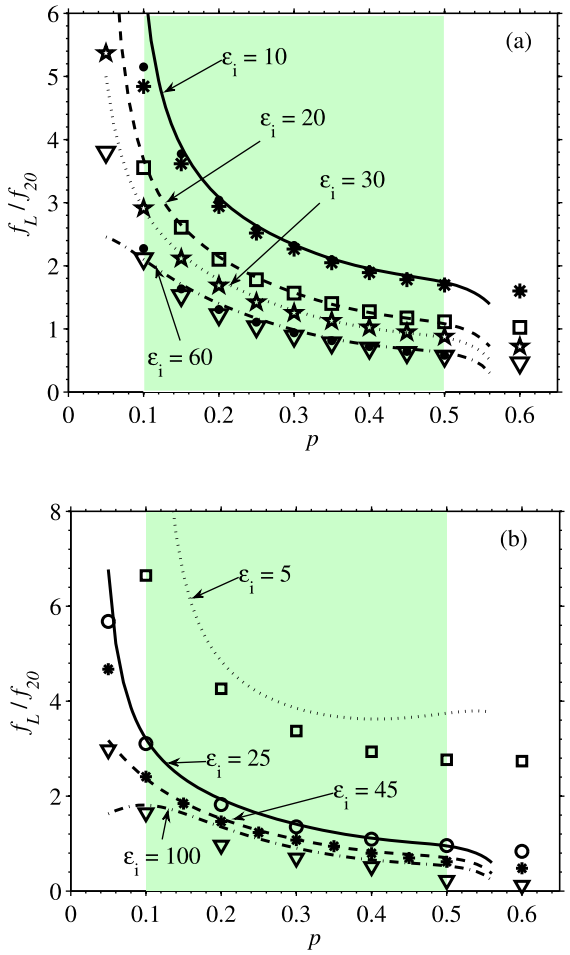

Figure 7. Evaluation of the interpolation function (15). All the curves denote the f_L/f_{20} calculated by (15); the markers other than the solid circles represent the f_L/f_{20} by (13); the solid circles denote the results by the first two terms of (13). (a) For fitting-involved p and ε_i. (b) For p and ε_i not employed in the data-fitting procedure.

where α_0' and α_2' are functions of p and ε_i. Let us now consider the limit f_L/f_{20}. Together with the defined 1% tolerance and (14), we have

$$\frac{f_L}{f_{20}} = \sqrt{\frac{1.01\varepsilon_{\mathrm{Ray}} - \alpha_0'}{\alpha_2'}}. \tag{15}$$

Finally, (15) is the established interpolation function to analyze the f_L/f_{20} for the composite slab in Figure 1 with the applicable range of $0.1 < p < 0.5$ and $10 < \varepsilon_i < 60$.

[26] Figure 7a compares the limit f_L/f_{20} by (15) with those by (13) for the composites with the fitting-involved p and ε_i. It is shown that the results by (15) have globally good agreement with those by (13), except when either a dilute composite or a small permittivity contrast is encountered. In these cases, the reduced accuracy of (15) is due to the fact that the corresponding α_2 is quantitatively as small as the fitting residual. Nevertheless, the limits f_L/f_{20} by (15) is shown to quickly converge to the more accurate references provided by (13) with the increasing p and ε_i.

[27] Besides the above fitting residuals, the errors due to the truncation of (13) are then evaluated. We add to Figure 7a the results by the first two terms of (13), illustrated by solid circles. These results are as expected slightly larger than those by (13), and overall have better agreement with those by (15). In particular, the difference between f_L/f_{20} by (13) and f_L/f_{20} by its first two terms is more noticeable for small p. Much weaker multipole interactions are expected when the composite becomes less concentrated, and α_4 should be very small as shown in Figure 6. However, the f_L/f_{20} in these cases is much larger so that the third term of (13) around f_L/f_{20} is larger for small p.

[28] To test the interpolation and extrapolation abilities of (15), we compare the f_L/f_{20} by (15) with those by (13) for the composites with p and ε_i, not employed to fit α_0 and α_2, both inside and outside the defined applicable range. It is illustrated in Figures 7a and 7b that (15) is capable of resolving a reasonable f_L/f_{20} within the applicable range. Once either p or ε_i is beyond this range, (15) gradually loses its accuracy, which indicates that a better fitting function for α_2 should be applied to further improve the accuracy of (15) and extend its applicable range in terms of p and ε_i.

[29] Finally, it is clearly demonstrated that with the increasing p and ε_i the dynamic trust region of the quasi-static estimate becomes narrower, i.e., the upper frequency limit f_L/f_{20} decreases. For a composite with a moderate permittivity contrast $\varepsilon_i/\varepsilon_e$ ($\leq$20), the quasi-static estimate can reasonably be applied when $f/f_{20} \leq 1.08$; that is, the ratio λ_{eff}/a is at least 18.5. If the whole applicable range of $0.1 < p < 0.5$ and $10 < \varepsilon_i < 60$ is considered, f/f_{20} should be smaller than 0.62, which means that the ratio λ_{eff}/a is at least 33.

5. Conclusion

[30] The quasi-dynamic homogenization of a geometrically simple dielectric-composite slab was considered in this paper with four different retrieval methods based on the simulated S parameters for oblique incidence. The BSCM was demonstrated as the most robust method; the applicability and the accuracy of the other methods using only parts of the transmission and reflection data are dependent on several parameters, e.g., the inclusion area fraction p, the relative permittivity ε_i of the inclusion, and the incident angle θ_0 of the plane wave.

[31] Based on the dispersive effective permittivities retrieved by the BSCM for a set of different p and ε_i, we developed an interpolation function to determine the upper frequency limit of the dynamic trust region of the quasi-static Lord Rayleigh formula, denoted as f_L/f_{20}, for the composite slab of our interest. It was confirmed that the proposed function can provide a reasonable prediction for f_L/f_{20} within an applicable range of $0.1 < p < 0.5$ and $10 < \varepsilon_i < 60$. To extend this range, a better model for the first dynamic correction term α_2 is required. It is finally shown that f_L/f_{20} will decrease with the increase of either p or ε_i, due to the stronger multipole interactions. Therefore, within the whole applicable range, the effective wavelength inside the material should be at least 33 times the edge length of the unit cell, so that the relative difference $(\varepsilon_{\mathrm{eff}} - \varepsilon_{\mathrm{Ray}})/\varepsilon_{\mathrm{Ray}}$ is not larger than 1%. The quasi-static estimate is then capable of describing the effective permittivity of the considered dielectric-composite slab reasonably.

[32] Finally, there could be an uncertainty in the effective thickness of the composite slab, since the effective medium-vacuum interface where reflection happens may differ from the natural boundary. Such an uncertainty was reported to have an effect on the sign of the imaginary parts of the retrieved parameters [*Chen et al.*, 2004]. Nevertheless, for lossless dielectric composites, the retrieved effective permittivities by the BSCM are practically purely real, which makes the sign-changing effect of the effective interface negligible. In addition, the proposed S parameter retrievals are applicable for dielectric composites with inclusions of any shape and/or with arbitrary permittivity contrast $\varepsilon_i/\varepsilon_e$. For instance, if the background vacuum is replaced by a dielectric material with relative permittivity ε_e different from unity, it becomes a natural way to choose the boundaries of the outermost layers as the medium-vacuum interface. Therefore, we neglect the effective interface effect and consider that the composite slabs are of their natural thicknesses.

Appendix A

[33] For α_0, the fitting function α_0' based on the Lord Rayleigh formula reads

$$\alpha_0' = b_1 + \frac{p}{b_2(\varepsilon_i+1)(\varepsilon_i-1)^{-1} - b_3 p - (\varepsilon_i-1)(\varepsilon_i+1)^{-1}(b_4 p^4 + b_5 p^8)}, \tag{A1}$$

where the optimized coefficients are: $b_1 = 1.00250316$; $b_2 = 0.50748121$; $b_3 = 0.53075173$; $b_4 = 3.14400420 \times 10^{-6}$; $b_5 = 0.80809230$.

[34] On the other hand, the applied fitting function α_2' for α_2 reads

$$\alpha_2' = q_{00} + q_{10}p + q_{01}\varepsilon_i + q_{20}p^2 + q_{11}p\varepsilon_i + q_{02}\varepsilon_i^2 + q_{30}p^3 + q_{21}p^2\varepsilon_i + q_{12}p\varepsilon_i^2, \tag{A2}$$

where the optimized coefficients are

$$\begin{pmatrix} q_{00} & q_{10} & q_{20} & q_{30} \\ q_{01} & q_{11} & q_{21} & q_{31} \\ q_{02} & q_{12} & q_{22} & q_{32} \end{pmatrix} = \begin{pmatrix} -0.00083963 & 0.00676935 & -0.02209411 & -0.00427475 \\ 2.18387320 \times 10^{-6} & 0.00032926 & 0.00323773 & 0 \\ 5.94057294 \times 10^{-7} & -8.70468344 \times 10^{-6} & 0 & 0 \end{pmatrix}. \tag{A3}$$

[35] **Acknowledgments.** This work was supported by the Academy of Finland and the Aalto University E.C.A. Faculty Graduate School.

References

Brosseau, C. (2006), Modelling and simulation of dielectric heterostructures: A physical survey from an historical perspective, *J. Phys. D Appl. Phys.*, *39*, 1277–1294, doi:10.1088/0022-3727/39/7/S02.

Chen, X., T. M. Grzegorczyk, B.-I. Wu, J. Pacheco, and J. A. Kong (2004), Robust method to retrieve the constitutive effective parameters of metamaterials, *Phys. Rev. E*, *70*, 016608, doi:10.1103/PhysRevE.70.016608.

Chen, X., B.-I. Wu, J. A. Kong, and T. M. Grzegorczyk (2005), Retrieval of the effective constitutive parameters of bianisotropic metamaterials, *Phys. Rev. E*, *71*, 046610, doi:10.1103/PhysRevE.71.046610.

Fietz, C., and G. Shvets (2010), Current-driven metamaterial homogenization, *Physica B*, *405*, 2930–2934, doi:10.1016/j.physb.2010.01.006.

Galek, T., K. Porath, E. Burkel, and U. van Rienen (2010), Extraction of effective permittivity and permeability of metallic powders in the microwave range, *Model. Simul. Mater. Sci. Eng.*, *18*, 025015, doi:10.1088/0965-0393/18/2/025015.

Kettunen, H., J. Qi, H. Wallén, and A. Sihvola (2010), Homogenization of dielectric composites with finite thickness, paper presented at the 26th Annual Review of Progress in Applied Computational Electromagnetics, Appl. Comput. Electromagn. Soc., Tampere, Finland.

Kong, J. A. (2008), *Electromagnetic Wave Theory*, EMW, Cambridge, U. K.

Landau, L. D., and E. M. Lifshitz (1984), *Electrodynamics of Continuous Media*, Pergamon, Oxford, U. K.

Levenberg, K. (1944), A method for the solution of certain non-linear problems in least squares, *Q. Appl. Math.*, *2*, 164–168.

Li, Z. F., K. Aydin, and E. Ozbay (2009), Determination of the effective constitutive parameters of bianisotropic metamaterials from reflection and transmission coefficients, *Phys. Rev. E*, *79*, 026610, doi:10.1103/PhysRevE.79.026610.

McPhedran, R., C. Poulton, N. Nicorovici, and A. Movchan (1996), Low frequency corrections to the static effective dielectric constant of a two-dimensional composite material, *Proc. R. Soc. London A*, *452*, 2231–2245, doi:10.1098/rspa.1996. 0119.

Milton, G. (2002), *The Theory of Composites*, Cambridge Univ. Press, Cambridge, U. K., doi:10.1017/CBO9780511613357.

Mochan, W. L., G. P. Ortiz, and B. S. Mendoza (2010), Efficient homogenization procedure for the calculation of optical properties of 3D nanostructured composites, *Opt. Express*, *18*, 22,119–22,127, doi:10.1364/OE.18.022119.

Nicolson, A. M., and G. F. Ross (1970), Measurement of the intrinsic properties of materials by time-domain techniques, *IEEE Trans. Instrum. Meas.*, *19*, 377–382, doi:10.1109/TIM.1970.4313932.

Qi, J., H. Kettunen, H. Wallén, and A. Sihvola (2010a), Different retrieval methods based on S-parameters for the permittivity of composites, paper presented at International Symposium on Electromagnetic Theory, Int. Union of Radio Sci., Berlin.

Qi, J., H. Kettunen, H. Wallén, and A. Sihvola (2010b), Compensation of Fabry-Pérot resonances in homogenization of dielectric composites, *IEEE Antennas Wirel. Propag. Lett.*, *9*, 1057–1060, doi:10.1109/LAWP.2010.2091103.

Rayleigh, L. (1892), On the influence of obstacles arranged in rectangular order upon the properties of a medium, *Philos. Mag.*, *34*, 481–502.

Sihvola, A. (1999), *Electromagnetic Mixing Formulas and Applications*, Inst. of Electr. Eng., London.

Silveirinha, M. G. (2007), Metamaterial homogenization approach with application to the characterization of microstructured composites with negative parameters, *Phys. Rev. B*, *75*, 115104, doi:10.1103/PhysRevB.75.115104.

Simovski, C. R., S. A. Tretyakov, A. H. Sihvola, and M. M. Popov (2000), On the surface effect in thin molecular or composite layers, *Eur. Phys. J. Appl. Phys.*, *9*, 195–204, doi:10.1051/epjap:2000105.

Sjöberg, D., and C. Larsson (2010), Characterization of composite materials in waveguides, paper presented at International Symposium on Electromagnetic Theory, Int. Union of Radio Sci., Berlin.

Smith, D. R., and J. B. Pendry (2006), Homogenization of metamaterials by field averaging, *J. Opt. Soc. Am. B Opt. Phys.*, *23*, 391–403, doi:10.1364/JOSAB.23.000391.

Smith, D. R., S. Schultz, P. Markoš, and C. M. Soukoulis (2002), Determination of effective permittivity and permeability of metamaterials from reflection and transmission coefficients, *Phys. Rev. B*, *65*, 195104, doi:10.1103/PhysRevB.65.195104.

Wang, B. N., J. F. Zhou, T. Koschny, M. Kafesaki, and C. M. Soukoulis (2009), Chiral metamaterials: Simulations and experiments, *J. Opt. A, Pure Appl. Opt.*, *11*, 114003, doi:10.1088/1464-4258/11/11/114003.

Weiglhofer, W. S., and A. Lakhtakia (2003), *Introduction to Complex Mediums for Optics and Electromagnetics*, SPIE Press, Bellingham, Wash., doi:10.1117/3.504610.

Weir, W. B. (1974), Automatic measurement of complex dielectric-constant and permeability at microwave-frequencies, *Proc. IEEE*, *62*, 33–36, doi:10.1109/PROC.1974.9382.

H. Kettunen, J. Qi, A. Sihvola, and H. Wallén, Department of Radio Science and Engineering, School of Electrical Engineering, Aalto University, PO Box 13000, FI-00076 Aalto, Finland. (qi.jiaran@tkk.fi)